Transient stimulated hyper-Raman scattering in an organic crystal

Q. Z. Wang, P. P. Ho, and R. R. Alfano
Institute for Ultrafast Spectroscopy and Lasers, Photonic Application Laboratory, Departments of Physics and Electrical Engineering, The City College and The Graduate School of the City University of New York, New York, New York 10031

R. Kashyap
British Telecom Research Laboratories, Martlesham Heath, Ipswich IP5 7RE, England
(Received 24 October 1991)

Transient stimulated hyper-Raman scattering has been observed in an ultrathin organic crystal (−)2-(α-methylbenzylamino)-5-nitropyridine (MBA-NP) pumped by picosecond laser pulses. Results were modeled by an instability theory.

PACS number(s): 42.65.−k

Future photonic devices will require optical materials that possess extremely large and fast nonlinear coefficients [1,2]. Nonlinear-optical materials based on π-conjugated organic materials have the potential to fulfill some of these basic requirements [3–8] for nonlinear-optical devices for communication and computation. The organic crystal (−)2-(α-methylbenzylamino)-5-nitropyridine (MBA-NP) has attracted much interest because of its extremely large $\chi^{(2)}$ and high optical damage threshold. In this paper, we report a nonlinear-optical effect of stimulated hyper-Raman scattering based on $\chi^{(5)}$ in an ultrathin MBA-NP crystal. Our observation, which arises from the interactions of two photons with the optical-phonon modes in submillimeter-thickness organic crystal, is different from previously stimulated hyper-Raman scattering observed in atomic or molecular vapor systems, which is attributed to transitions between electronic states [9–14].

A typical nonlinear spectrum from ultrathin 600-μm MBA-NP crystal under 1054-nm, 10-ps pulse excitation is displayed in Fig. 1(a). The salient feature of the curve displayed indicates that there are four distinct maxima located at 527 nm [second-harmonic generation (SHG)], 556 nm, 351 nm [third-harmonic generation (THG)], and 364 nm. The two new spectral features are located at 556 and 364 nm, which are shifted by 992 cm^{-1} from SHG and THG signals, respectively. However, there was no observable stimulated signals in the infrared region due to absorption. Figure 1(b) displays the ir spectrum of a 40-μm-thick MBA-NP crystal and the spontaneous Raman spectrum of a MBA-NP crystal pumped by a 80-mW cw argon laser at 488 nm. The ir spectrum was measured with a FTS-40 Digilab fast Fourier transform ir spectrometer system. The Raman signal was detected by an optical multichannel analyzer system (EG&G) in combination with a Triplemate monochromator (Spex Industries Inc.). The ir spectrum shows that the mode at 992 cm^{-1} is ir active.

Figure 2 shows the intensity dependence of hypersignal at $2\nu-\nu_p$ (556 nm) with the 1054-nm pump intensity. The signal intensity at 556 nm increases rapidly and saturates as shown in Fig. 2.

The temporal behavior of the SHG at 527- and 556-nm signals of the 1054-nm laser pulse passing through a 1.9-cm-long MBA-NP crystal have been measured by a 2-ps resolution streak camera and are displayed in Fig. 3. The SHG signal has two separate peaks in time generated from the entrance and exit surfaces, respectively. This signal is due to the phase mismatching and the interference of the signals generated in different positions [15]. Only a sharp peak in time at 556 nm generated from the exit end of the crystal can be observed. This feature is a clear signal of stimulated emission pulse. The temporal distributions of the SHG and 556-nm signals generated from 600-μm MBA-NP are similar. Both have one clear peak with the pulse duration about the same as that of the pump pulse.

One key characteristic of the measured nonlinear spectral signal is that the intensity ratio of I_{556}/I_{527} is almost equal to I_{364}/I_{351} under an input 1054-nm intensity change from 3×10^9 to 5×10^{10} W/cm^2. The intensities at 556 and 364 nm are about one-tenth of the intensities at 527 and 351 nm, respectively. The signal intensity of SHG frequency 527 nm varies as $I_{2\nu}\propto I_\nu^2$. The signal intensity at THG is found to be almost linearly to that at SHG. Phase-matched second-harmonic generation was not observed which may be accounted for by the poor quality of the sample and orientation.

The signal at 3ν can arise from both the third-harmonic generation ($\propto\chi^{(3)}$) and the three-wave mixing ($\propto\chi^{(2)}$). To find out which signal generating process is responsible for 3ν, both transmission and reflection methods were performed. Our experimental results indicates that the intensity at 3ν is linearly proportional to the intensity at 2ν for both cases when the input laser intensity at 1054 nm was high and kept constant. These observations indicate that the signal at 3ν mainly originates from the three-wave mixing via $\chi^{(2)}$ from signals at 2ν and ν. It was estimated experimentally that about less than 10% of the intensity of the signal at 3ν was generated from THG through $\chi^{(3)}$. The absorption depths of both MBA-NP and ZnSe are comparable to the coherence length. A standard model of THG [16,17] was used to estimate the value of the third-order susceptibility of

MBA-NP. It was found that the $\chi^{(3)}$ of MBA-NP is less than 1% of that of ZnSe, about the order of 10^{-13} esu.

From experiments, the signals at frequency $3\nu-\nu_p$ mostly arises from the three-wave mixing with strong signals at ν and $2\nu-\nu_p$ through $\chi^{(2)}$. The signal intensity at $3\nu-\nu_p$ was found to vary as $I_{3\nu-\nu_p} \propto (\chi^{(2)})^2 I_\nu I_{2\nu-\nu_p}$. Therefore, the ratio of the intensity at $2\nu-\nu_p$ to the intensity at 2ν is identical to the ratio of $3\nu-\nu_p$ to 3ν,

$$\frac{I_{3\nu-\nu_p}}{I_{3\nu}} = \frac{(\chi^{(2)})^2 I_\nu I_{2\nu-\nu_p}}{(\chi^{(2)})^2 I_{2\nu} I_\nu} = \frac{I_{2\nu-\nu_p}}{I_{2\nu}} .$$

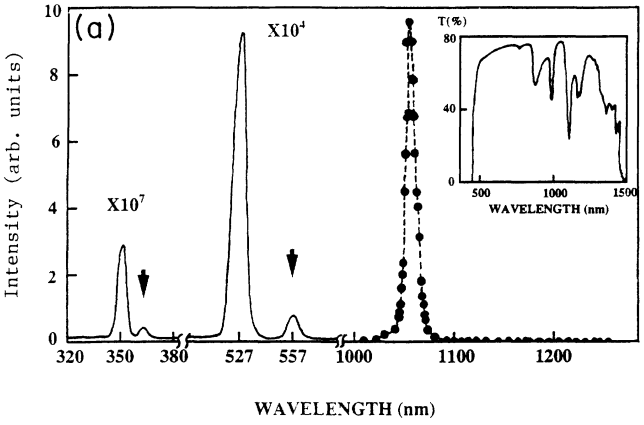

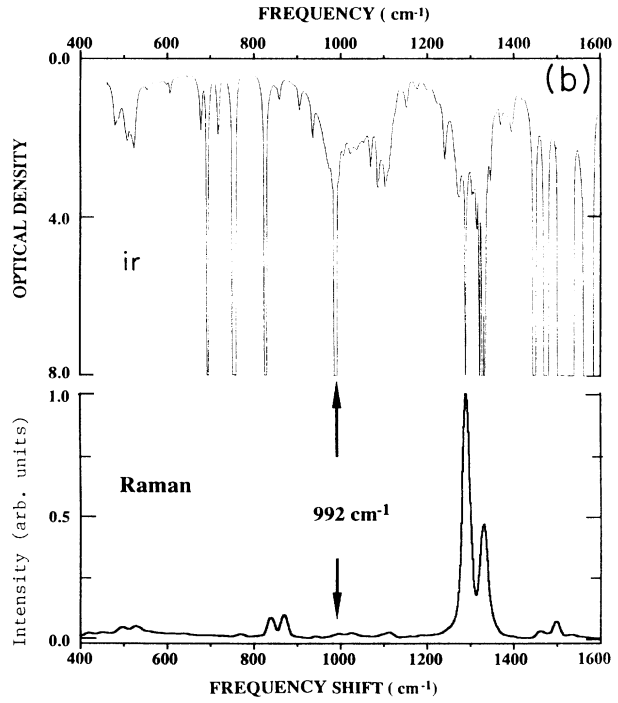

FIG. 1. (a) Nonlinear signals from 600-μm MBA-NP in ultraviolet and visible spectral regions generated by 1054-nm, 8-ps laser pulses. Arrows point to the observed salient features. The intensities from 330 to 370 nm and from 500 to 600 nm displayed in Fig. 1 have been multiplied by 10^7 and 10^4, respectively, for the comparison of the pump-laser intensity. The inset shows the absorption curve of a 1.9-cm MBA-NP crystal. (b) ir absorption spectrum of MBA-NP with 40-μm thickness and Raman spectrum of a MBA-NP crystal pumped by a cw laser at 488 nm.

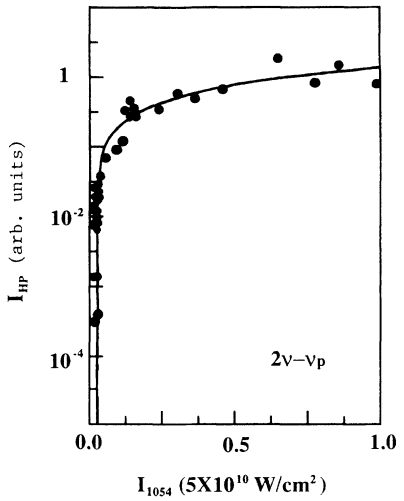

FIG. 2. Intensity dependence of output intensity at frequency $2\nu-\nu_p$ from ultrathin MBA-NP. The solid line is calculated from Eq. (6) using $\beta_p=0.7$ cm^{-1}, $\gamma=10^{-4}$, and $I_c/\gamma=1.67\times10^9$ W/cm^2. There is no observable optical damage in MBA-NP with over 500 shots of 10-ps laser pulses with peak intensity up to 50 GW/cm^2.

Besides the possibility of the stimulated hyper-Raman scattering [12–17] for our observed signal generated at $2\nu-\nu_p$, there may be three other possibilities: (1) the stimulated Raman scattering via 2ν; (2) second-harmonic generation of the stimulated Raman of the pump laser; (3) parametric hyper-Raman generation of the incident laser ν and its stimulated Raman scattering ($\nu_p=992$ cm^{-1}) at $1/(\nu-\nu_p)=1177$ nm. However, the later three possibilities can be ruled out by the following experimental results.

When an external 527-nm laser pulse with an intensity comparable to the SHG generated by 1054 nm passed through the MBA-NP crystal, no signal at $2\nu-\nu_p$ was observed. When the incident intensity of the primary pumping laser was kept constant, the output intensity at $2\nu-\nu_p$ remained almost constant when the intensity at 2ν was changed externally. In addition, no significant Raman signal at 992 nm^{-1} was observed in the spontaneous Raman spectrum. These observations rule out the first possibility. Due to the ir absorption in the possible Raman line region, no strong stimulated Raman of the pump laser for 600-μm-thick MBA-NP crystal was observed as shown in Fig. 1. This is the key factor to the observation of stimulated hyper-Raman scattering. The lack of the stimulated Raman scattering of the primary pump laser in the ir region makes the stimulated hyper-Raman scattering the first nonlinear process in the MBA-NP crystal pumped by 1054-nm laser pulses. Furthermore, there was no sinusoidal oscillation, which is the typical feature of the signal from frequency upconversion parametric process, in the temporal distribu-

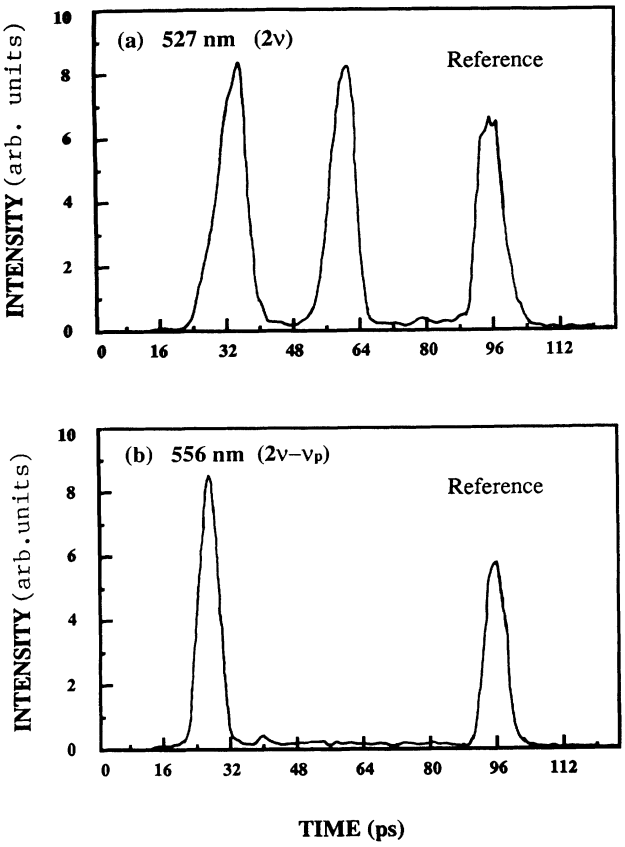

FIG. 3. Temporal behavior of the nonlinear signals generated from a 1.9-cm-long MBA-NP crystal. (a) SHG signal at 527 nm (2ν); (b) hyper-Raman signal at 556 nm ($2\nu-\nu_p$).

tion of the signal at 556 nm. These ruled out the second and third possibilities. The ir absorption spectrum shows that there is a strong absorption band about $\nu_p=992$ cm^{-1}. Therefore, the signal at $2\nu-\nu_p$ appears to arise from hyper-Raman scattering of the primary pump laser.

A parametric instability theory introduced by Sparks [18] for stimulated Raman scattering is modified to quantitatively explain intensity dependence of the hyper-Raman signal at $2\nu-\nu_p$. Using the standard perturbation theory results for the transition rate between energy states, the equation of motion for the hyper-Raman-photon and phonon occupation numbers $n_{\rm HR}$ and n_p are given as follows:

$$\frac{\partial n_{HL}}{\partial t}=C[(n_{\rm HR}+n_p+V^{-1})n_{L\rm eff}^2 -2n_{\rm HR}n_pn_{L\rm eff}-n_{\rm HR}n_pV^{-1}] -v\alpha_{\rm HR}n_{\rm HR}-v\frac{\partial n_{\rm HR}}{\partial x}\ , \tag{1}$$

and

$$\frac{\partial n_p}{\partial t}=C[(n_{\rm HR}+n_p+V^{-1})n_{L\rm eff}^2 -2n_{\rm HR}n_pn_{L\rm eff}-n_{\rm HR}n_pV^{-1}] -\Gamma_p(n_p-\bar{n}_p)-v_p\frac{\partial n_p}{\partial x}\ , \tag{2}$$

where $n_{L\rm eff}$ is the effective photon occupation number of laser participating in the hyper-Raman scattering process in the medium, $C=2\pi|V_{\rm HR}/\hbar|^2V^3\delta(\nu)$, with $V_{\rm HR}$ the equivalent hyper-Raman matrix element including the contributions from parametric hyper-Raman scattering, $\alpha_{\rm HR}$ the absorption coefficient, V the volume of the sample, the argument of the $\delta\nu\equiv 2\nu_L-\nu_{\rm HR}-\nu_p$, v is the velocity of the hyper-Raman light in the medium, α the absorption coefficient, v_p is the phonon velocity, $\bar{n}_p$ is thermal-equilibrium value of n_p, and Γ_p is the inverse lifetime of phonon n_p.

The intensities of laser and hyper-Raman scattering are $I_L=\hbar\nu_Lc_Ln_L$ and $I_{\rm HR}=\sum_M\hbar\nu_{\rm HR}vn_{\rm HR}$, where the sum is over the hyper-Raman modes M and c_L the velocity of the laser. Dispersion is neglected where $c_L=v$.

Assuming $n_p\gg V^{-1}$ and $n_p\gg n_{\rm HR}$, Eq. (2) reduces to

$$\frac{\partial}{\partial t}(n_p-\bar{n}_p)=\Gamma_p\left[n_p\frac{n_{L\rm eff}^2}{n_c}-(n_p-\bar{n}_p)\right]\ , \tag{3}$$

where $n_c=(\Gamma_p/C)^{1/2}$ is the critical value of n_i. It can be seen from Eq. (3) that when the effective laser pumping densities is greater than n_c, the phonon density n_p becomes unstable since $\partial(n_p-\bar{n}_p)/\partial t>0$ for all $\bar{n}_p$. From the experimental point of view it follows that at a certain critical effective laser density $I_c=\hbar\omega_Ln_c$, an explosive build up of the phonon occupation number n_p, can take place. The increase in phonons causes a similar increase in the hyper-Raman Stokes radiation intensity.

Since the hyper-Raman scattering is a three-photon process in which a system is excited with two photons of laser at ν_L and emits one photon at the frequency $2\nu_L-\nu_p$, the effective photon occupation number of the laser can be written as

$$n_{L\rm eff}=\gamma n_i-2\sum_M n_{\rm HR}\ , \tag{4}$$

where n_i is the total photon occupation number of incident laser pulse, and the saturation coefficient γ is the effective coefficient of photons of the laser participating in the hyper-Raman scattering process depending on the total phonon modes, the intrinsic properties of material, and the pump-laser intensity. As a first-order assumption, we take γ as a constant for a small change of pump-laser intensity in our later calculation. Substituting Eq. (4) into Eqs. (1) and (2), the equation of motion for $n_{\rm HR}$ in a steady-state case can be written as

$$\left[\frac{dn_{\rm HR}}{dx}+\alpha_{\rm HR}n_{\rm HR}\right]\left[n_{Lc}^2-\left[\gamma n_i-2\sum_M n_{\rm HR}\right]^2+2n_{\rm HR}\left[\gamma n_i-2\sum_M n_{\rm HR}\right]\right]=\beta_p\left[(n_{\rm HR}+\bar{n}_p)\left[\gamma n_i-2\sum_M n_{\rm HR}\right]^2 -2n_{\rm HR}\bar{n}_p\left[\gamma n_i-2\sum_M n_{\rm HR}\right]\right]\ , \tag{5}$$

where $\beta_p=\Gamma_p/v$. Since the phonon velocity v_p and value of one phonon per volume V are small, the last term in Eq. (2) and the terms with V^{-1} have been neglected in the derivation of Eq. (5).

As the first-order approximation $\sum_M n_{\rm HR}$ in Eq. (5) can be formly replaced by Mn, where M is the number of effective modes and n is the average value of the hyper-Raman-photon occupation number in each mode. Equation (5) reduces to

$$\frac{dI_{\rm HR}}{dx}=\beta_P\frac{(I_{\rm HR}+I_{sp})(\gamma I_i-I_{\rm HR})^2-I_{\rm HR}I_{sp}(\gamma I_i-I_{\rm HR})/M}{I_c^2-(\gamma I_i-I_{\rm HR})^2+I_{\rm HR}(\gamma I_i-I_{\rm HR})/M}-\alpha_{\rm HR}I_{\rm HR}\ , \tag{6}$$

where $I_{\rm HR}=\hbar\omega_{\rm HR}Mn$, $I_{sp}=\hbar\omega_{\rm HR}M\bar{n}_p$, and $I_i=\hbar\omega_L n_i$.

A numerical method is used to solve Eq. (6) for the general case. When $I_{\rm HR}$ is much smaller than I_i, the explicit solution to Eq. (6) is

$$I_{\rm HR}\sim I_{sp}[\exp(gx)-1]+I_{\rm HR}(0)\exp(gx)\ , \tag{7}$$

where $g=\beta_p(\gamma I_i)^2/[I_c^2-(\gamma I_i)^2]$ with γ the saturation coefficient. The first term on the right-hand side of Eq. (7) is the amplified spontaneous emission of hyper-Raman and the second term is stimulated hyper-Raman scattering. When $\beta x\ll 1$ and $I_{\rm HR}(0)=0$, then $I_{\rm HR}\sim I_{sp}\beta_p x I_L^2 x$, which is the result of the spontaneous hyper-Raman intensity [19].

In Fig. 2 the experimental results on the intensity dependence of hyper-Raman scattering is fitted using Eq. (6) as the solid line. In the calculation, the value of $\beta_p=0.7\ \ {\rm cm}^{-1}$ was used which corresponds to $\Gamma^{-1}\sim 10^{-11}$ s. It was estimated from the experiment that the saturation coefficient $\gamma\sim 10^{-4}$. By adjusting the value of I_c, excellent agreement has been achieved over five decades between the theoretical calculation and the experimental results when input laser intensity is higher than 1×10^9 W/cm^2. When the laser intensity was lower than 1×10^9 W/cm^2, the hyper-Raman signal reduced to level 10^{-6} of the saturation value which is below our experimental sensitivity.

In conclusion, experimental measurement and theoretical analysis support the observation of transient stimulated hyper-Raman scattering in a thin MBA-NP crystal.

We gratefully acknowledge useful discussions with Peixuan Ye and J. Buchert. We thank A. Woodward for his help in performing the ir spectrum measurement and Gezhi Weng for her assistance in taking the Raman spectrum. This research is supported in part by grants from Hamamatsu Photonics K. K. and the Professional Staff Congress/Board of Higher Education.

[1] R. Terhune and D. Weinberger, J. Opt. Soc. Am. B **4**, 661 (1987).
[2] R. Kashyap, J. Opt. Soc. Am. B **6**, 313 (1988).
[3] E. Garmire, *Physics of Quantum Electronics,* edited by P. L. Kelley, B. Lax, and P. E. Tannenwald (McGraw-Hill, New York, 1966).
[4] B. F. Levine, Chem. Phys. Lett. **37**, 516 (1976).
[5] P. P. Ho, N. L. Yang, T. Jimbo, Q. Z. Wang, and R. R. Alfano, J. Opt. Soc. Am. B **4**, 1025 (1987).
[6] R. T. Bailey, F. R. Cruickshank, S. M. G. Guthrie, B. J. McArdle, H. Morrison, D. Pugh, E. A. Shepherd, J. N. Sherwood, C. S. Yoon, R. Kashyap, B. K. Nayar, and K. I. White, Opt. Commun. **65**, 229 (1988).
[7] H. Kanbara, H. Kobayashi, and K. Kubodera, IEEE Photon Tech. Lett. **1**, 149 (1989).
[8] R. Bailey, F. Cruickshank, S. Guthrie, B. McArdle, H. Morrison, D. Pugh, E. Shepherd, J. Sherwood, and C. Yoon, J. Mod. Opt. **35**, 511 (1988).
[9] S. Yatsiv, M. Rokni, and S. Barak, IEEE J. Quantum Electron. **QE-4**, 900 (1968).
[10] Q. H. F. Vrehen and H. M. J. Hikspoors, Opt. Commun. **21**, 127 (1977).
[11] D. Cotter, D. C. Hanna, W. H. W. Tuttlebee, and M. A. Yuratich, Opt. Commun. **22**, 190 (1977).
[12] J. Reif and H. Walther, Appl. Phys. **15**, 361 (1978).
[13] D. Krokel, K. Ludewigt, and H. Welling, IEEE J. Quantum Electron. **QE-22**, 489 (1986).
[14] U. Czarnetzki, U. Wojak, and H. F. Dobele, Phys. Rev. A **40**, 6120 (1989).
[15] P. P. Ho, D. Ji, Q. Z. Wang, and R. R. Alfano, J. Opt. Soc. Am. B **7**, 276 (1990).
[16] *CRC Handbook of Laser Science and Technology,* edited by M. Weber (CRC, Boca Raton, FL, 1986), Vol. III.
[17] J. Reintjes, *Nonlinear Optical Parametric Processes in Liquids and Gases* (Academic, New York, 1984).
[18] M. Sparks, Phys. Rev. Lett. **32**, 450 (1974).
[19] V. N. Denisov, B. N. Mavrin, and V. B. Podobedov, Phys. Rep. **151**, 1 (1987).